Revival of Electron Coherence in a Quantum Wire of Finite Length

Jaeuk U. Kim,[1] W.-R. Lee,[1] Hyun-Woo Lee,[2] and H.-S. Sim[1,*]

[1]*Department of Physics, Korea Advanced Institute of Science and Technology, Daejeon 305-701, Korea*
[2]*PCTP and Department of Physics, Pohang University of Science and Technology, Pohang, Kyungbuk 790-784, Korea*
(Received 25 August 2008; published 17 February 2009)

We study the spatial decay of electron coherence due to electron-electron interaction in a finite-length disorder-free quantum wire. Based on the Luttinger liquid theory, we demonstrate that the coherence length characterizing the exponential decay of the coherence can vary from region to region, and that the coherence can even revive after the decay. This counterintuitive behavior, which is in clear contrast to the conventional exponential decay with single coherence length, is due to the fractionalization of an electron and the finite-size-induced recombination of the fractions.

DOI: 10.1103/PhysRevLett.102.076401 PACS numbers: 71.10.Pm, 03.65.Yz, 73.23.−b, 85.35.Ds

Introduction.—Quantum coherence of a particle wave is responsible for various quantum phenomena. Conventionally, the coherence of a particle decays exponentially with time due to scattering with other particles. This decay "law" was observed experimentally in electron interferometers [1,2], where the interference visibility decays as e^{-L/ℓ_ϕ} with the length L of the interference path. Here constant ℓ_ϕ is often called the coherence length, since the visibility represents how well the coherence is preserved during the electron propagation along the path [3].

Electron-electron interaction is known as a dominant scattering source that induces the decay of the electron coherence (dephasing) at low temperature. The interaction generates nontrivial effects [4–8]. For instance, when an electron is injected to an infinitely long one-dimensional wire, the interaction splits it into two fractional charges [4]. The charge fractionalization was experimentally detected [5], and is responsible [6] for the exponential decay of the coherence in the infinite wire.

In this Letter, we consider a *finite* one-dimensional wire and find surprising deviations from the infinite case in the temperature regime where the thermal energy is comparable to or larger than the discrete level spacing due to the finite-size effect. The coherence length characterizing the exponential decay of the coherence can vary from region to region, even though the wire is homogeneous, and moreover the coherence can even revive after the decay. We attribute this counterintuitive behavior to the interaction-induced fractionalization of electrons [4,5] and to the separation and recombination of the fractions in the finite-length wire. This demonstrates that electron-electron scattering does not occur in a random phase-averaging fashion, and clarifies the nature of the coherence of interacting particles.

Interferometer.—We consider an electron interferometer (Fig. 1), in which a disorder-free wire of length L weakly couples to two bulk electrodes at two positions x_i and x_e via electron tunneling. For simplicity, we ignore the spin degree of freedom for a while, and neglect the interaction in the electrodes. The total Hamiltonian of the setup is written as $H = H_{\rm wire} + H_L + H_R + H_t$, where $H_{L(R)}$ is the Hamiltonian of the noninteracting left (right) electrode, $H_t = [\gamma_1 \Psi^\dagger(x_i)\Psi_L(0) + \gamma_2 \Psi_R^\dagger(0)\Psi(x_e) + \gamma_3 \Psi_R^\dagger(0)\Psi_L(0) + {\rm H.c.}]$ describes the tunneling, $\Psi_{L(R)}(0)$ is the electron field operator at the tunneling point of the left (right) electrode, and γ_1, γ_2, γ_3 are the tunneling amplitudes along the interference loop. The electron field operator $\Psi(x)$ at position x in the wire satisfies $\Psi(0) = \Psi(L) = 0$ at the wire boundaries. The Hamiltonian $H_{\rm wire}$ of the wire will be given later.

In the setup, under bias voltage V, electron current flows between the electrodes via two paths, the direct tunneling (γ_3) and the elastic cotunneling ($\gamma_1\gamma_2$) through the wire, which cause the interference. We derive the interference parts $I_{\rm int}$ of the current, $I_{\rm int}(x_i, x_e) \propto {\rm Re}[\gamma_1\gamma_2\gamma_3^*] \times \mathcal{P}\int d\omega d\omega' A(x_i, x_e; \omega)\{[f_L(\omega') - f_R(\omega')]/(\omega' - \omega)\}$, by using the Keldysh Green function [9,10] and retaining the perturbation series up to the lowest order in the tunneling amplitudes (e.g., for $\gamma_1 \gg \gamma_2, \gamma_3$). Here $\mathcal{P}$ means the principal value of the integral, $f_{L(R)}$ is the Fermi distribution function of the left (right) electrode, and $A(x_i, x_e; \omega)$ is a propagator through the wire (introduced below). The above derivation is valid for any specific form of $H_{\rm wire}$.

In the linear response regime, we obtain the interference part $G_{\rm int} \equiv dI_{\rm int}/dV$ of the differential conductance,

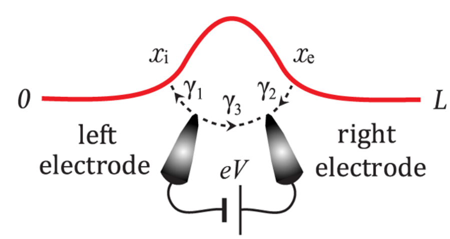

FIG. 1 (color online). Electron interferometer, consisting of a disorder-free one-dimensional wire of length L and two electrodes. Electron tunneling occurs between the left (right) electrode and the injection position x_i (extraction x_e) of the wire, and between the electrodes; see dashed arrows.

$$G_{\rm int}(x_i, x_e) \propto {\rm Re}[\gamma_1 \gamma_2 \gamma_3^*] \int_0^\infty dt F_T(t) {\rm Im}[A(x_i, x_e; t)]. \quad (1)$$

Here $A(x_i, x_e; t) \equiv \langle \Psi^\dagger(x_i, 0)\Psi(x_e, t) + \Psi(x_e, t)\Psi^\dagger(x_i, 0)\rangle_w$ is the Fourier transform of $A(x_i, x_e; \omega)$ and represents the electron propagation amplitude in the wire from x_i to x_e during the time interval t, and $\langle \cdots \rangle_w$ denotes the average over the equilibrium states of the wire for $\gamma_1 = \gamma_2 = 0$. The weighting factor, $F_T(t) = \pi k_B T t/[\hbar \sinh(\pi k_B T t/\hbar)]$, which smears out the interference, comes from the thermal distribution $f_{L/R}$ of electrons in the electrodes and from the elastic cotunneling weight $1/(\omega' - \omega)$; k_B is the Boltzmann constant, T is the temperature, and $\hbar$ is the Planck constant divided by 2π. The thermal smearing is more pronounced for longer t, as $F_T(t)$ decays rapidly as $e^{-\pi k_B T t/\hbar}$ for $t \gg \hbar/(k_B T)$.

All the interaction effects on the coherence are contained in $A(x_i, x_e; t)$. We consider a short-range repulsive interaction. We evaluate A (thus $G_{\rm int}$) by using the bosonization technique [11–13], a reliable nonperturbative treatment in the low energy regime. After the bosonization [12], the Hamiltonian of the wire becomes $H_{\rm wire} = \epsilon \sum_{q>0} n_q b_q^\dagger b_q + \hbar\pi v N^2/(2gL)$, where the boson operator $b_q^\dagger$ ($[b_q, b_{q'}^\dagger] = \delta_{q,q'}$) creates a plasmon with wave vector $q = \pi n_q/L$ ($n_q = 1, 2, \ldots$) and the operator N counts the number of excess electrons in the wire. Here $\epsilon = \pi\hbar v/L$ is the plasmon level spacing, $v = v_F/g$ is the plasmon propagation velocity, v_F is the bare Fermi velocity, and g is the Luttinger parameter describing the interaction strength; $g = 1$ in the noninteracting case and g decreases toward 0 for more repulsive interaction. The first term of $H_{\rm wire}$ comes from the plasmon excitations, while the second comes from the zero-mode fluctuations.

Revival of coherence and multiple coherence lengths.—At temperature $k_B T \gtrsim \epsilon$ (the range we focus on), one might expect that the electron coherence in the finite wire shows the same exponential decay as in an infinite wire [6], as the finite level spacing ϵ is masked by $k_B T$. However, our result (Fig. 2), obtained from the bosonization and Eq. (1), shows that finite-size effects persist even in this relatively high temperature regime: Although $G_{\rm int}$ follows the exponential decay form $e^{-|x_e - x_i|/\ell_\phi}$, the coherence length ℓ_ϕ changes from region to region. Moreover $G_{\rm int}$ can even have a peak at a special position $x_e = L - x_i$, showing the revival of the coherence.

An insight into this striking behavior can be obtained from the bosonization form of the electron field operator $\Psi(x)$. For this purpose, we decompose $\Psi(x)$ into right-moving (ψ_+) and left-moving (ψ_-) fields, $\Psi(x) = \psi_+(x) + \psi_-(x)$, where $\psi_\pm(x) = (\mp i/\sqrt{2L})\sum_{k>0} e^{\pm ikx} c_k$. Here $c_k^\dagger$ creates an electron with wave vector $k = \pi n_k/L$ ($n_k = 1, 2, \ldots$) in the wire and satisfies $\{c_k, c_{k'}^\dagger\} = \delta_{k,k'}$. The time evolution of ψ_+ has the bosonized form [12],

$$\psi_+(x, t) \to \frac{e^{i(k_F + \pi/2L)x}}{\sqrt{2\pi a}} e^{i\phi_0(x,t)} e^{i[c_+\varphi(x - vt) + c_-\varphi(-x - vt)]}.$$

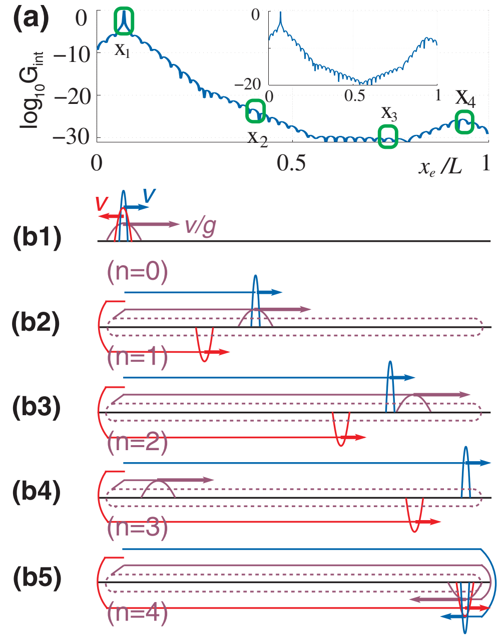

FIG. 2 (color). Revival of coherence. (a) Plot of $\log_{10}|G_{\rm int}|$, as a function of x_e, for the spinless case with $x_i = 0.07L$, $k_B T = 5\epsilon$, $g = 1/7$, and Fermi wave vector $k_F = 40\pi/L$. The interference signal $G_{\rm int}(x_i, x_e)$ follows the exponential decay of $\exp(-|x_e - x_i|/\ell_\phi)$ with *multiple* coherence lengths ℓ_ϕ as x_e moves from x_i, and it *revives* around $x_e = L - x_i$. $G_{\rm int}$ is normalized by the value at $x_e = x_i$ and oscillates with period $2\pi k_F^{-1}$. Inset: $\log_{10}[|G_{\rm int}|\exp(|x_e - x_i|/\ell_{\phi,T})]$. In this plot, the pure thermal phase smearing is factored out. (b1)–(b5) Schematic views of the dynamics of the three modes (depicted by blue, red, and purple), generated at x_i and time $t = 0$ by the injection of an electron to the wire considered in (a). The modes move with different velocities ($\pm v$ and v/g) and are bounced at the wire boundaries. In (b1)–(b4), the blue mode arrives at x_j at time $t_j = (x_j - x_i)/v$, $j = 1, 2, 3, 4$, moving from x_i to x_j without any bounce, while in (b5) it arrives at x_4 at $t_5 = (2L - x_4 - x_i)/v$ after one bounce at the right boundary. Here, $x_1 = x_i$, $x_2 = 0.4L$, $x_3 = 0.75L$, and $x_4 = L - x_i$ are selected. At each time, the purple mode has experienced n times of the round trip (the dashed purple line) with length $2L$. The mode configurations at time t_j dominantly contribute to $G_{\rm int}(x_i, x_j)$, and the configurations at t_4 and t_5 result in the revival of the coherence.

Here, $\phi_0(x, t) = \pi(x - g^{-1}vt)N/L - \chi$ is the fermionic zero mode, coming from the thermal fluctuation of the number of electrons occupying the wire, $c_+\varphi(x - vt)$ and $c_-\varphi(-x - vt)$ are the bosonic plasmon modes, $[\chi, N] = i$, $c_\pm = (g^{-1/2} \pm g^{1/2})/2$, $\varphi(z) = \sum_{q>0}\sqrt{\pi/qL} \times e^{iqz - aq/2} b_q + {\rm H.c.}$, and a is the usual short-distance cutoff. Note that $\psi_-(x, t)$ has a similar expression. According to this description, when an electron tunnels into $\psi_+(x_i)$, it breaks into three fractions in the spinless case, one right-moving plasmon mode $c_+\varphi$ (the blue mode of Fig. 2), another left-moving plasmon mode $c_-\varphi$ (red), and one right-moving zero mode ϕ_0 (purple); there is also the tunneling into $\psi_-(x_i)$, which has the same fractionalization but with "left" and "right" exchanged. The two plasmon modes move with the same speed v, while the zero mode moves with v/g; in the noninteracting case ($g = 1$), no fractionalization occurs, as the blue and the zero mode move together and the red disappears ($c_- = 0$). Because of bounces at the wire boundaries, the modes separate and recombine repeatedly. The overlap between the modes at time t and the electron state localized at x_e determines $A(x_i, x_e; t)$. The overlap becomes larger as the modes locate closer to x_e, and is drastically enhanced when some of the modes recombine at x_e, which is responsible for the nontrivial behavior of the coherence.

We first examine the contribution of the two plasmon modes to the coherence. Hereafter we choose $x_i \in [0, L/2]$ without loss of generality. The contribution is negligible except for around the times when the blue mode arrives at x_e, since the blue has a bigger effect on the overlap than the red ($c_+ > c_-$). In view of the decay in $F_T(t)$ with time t, we first consider the shortest one among those special times, namely, $t_{\rm dire} = |x_e - x_i|/v$ at which the blue mode propagates from x_i to x_e directly without any boundary bounce [Figs. 2(b1)–2(b4)]. The magnitude of the contribution from $t_{\rm dire}$ depends on the separation distance between the blue and red modes at $t_{\rm dire}$. A natural candidate of the distance is $d_1 = 2vt_{\rm dire}$. In addition to d_1, we have another candidate, $d_2 = 2L - 2vt_{\rm dire}$, which comes from the fact that the two modes recombine at $t = L/v$ ($>t_{\rm dire}$) after their boundary bounces [Fig. 2(b5)]. The smaller of d_1 and d_2 determines the magnitude of the contribution. For $x_e \lesssim L/2 + x_i$, d_1 ($<d_2$) increases with x_e, while d_2 ($<d_1$) decreases for $x_e \gtrsim L/2 + x_i$. Thus the contribution from $t_{\rm dire}$ decreases and then increases as x_e moves from x_i toward L.

The second shortest time is $t_{\rm boun} = (2L - x_i - x_e)/v$ [or $t_{\rm boun} = (x_i + x_e)/v$ if the blue moves to the left], at which time the blue mode arrives at x_e after one bounce at a wire boundary. Because of $F_T(t)$, the contribution from $t_{\rm boun}$ suffers larger thermal smearing than that from $t_{\rm dire}$. Unlike $t_{\rm dire}$, however, the red mode also arrives at x_e (recombines with the blue) if $x_e = L - x_i$, enhancing $A(x_i, x_e; t)$ drastically [Fig. 2(b5)]. Thus around $x_e = L - x_i$, the contributions from $t_{\rm dire}$ and $t_{\rm boun}$ can compete. For smaller g and x_i (closer to wire boundaries), we find that $t_{\rm boun}$ becomes more important. In Fig. 2, $t_{\rm boun}$ ($t_{\rm dire}$) is more important for $x_e \gtrsim L - x_i$ ($x_e \lesssim L - x_i$). Both the events at $t_{\rm dire}$ and $t_{\rm boun}$ result in the revival of the coherence around $x_e = L - x_i$ due to the recombination.

Next we examine the contribution of the zero mode, which is determined by its overlap with the blue mode at the time it arrives at x_e. Since the zero mode moves faster than the blue by factor $1/g$ (>1), the overlap decays with time right after the electron injection into the wire. When x_e is sufficiently away from x_i, however, it now becomes possible that the zero mode makes the round trip of the wire once and recombines with the blue mode [Fig. 2(b2)], which will suppress the decay. This recombination and the contribution from the two plasmon modes together result in the coherence length near $x_e = x_2$ [Fig. 2(a)], which is different from the coherence length near $x_e = x_i$. For sufficiently small g, the zero mode experiences the round trip multiple times, while the blue mode moves directly from x_i to $L - x_i$. Then, the recombination between the zero mode and the blue can occur at multiple locations. These multiple recombinations, together with the contributions from the two plasmon modes, give rise to the multiple coherence lengths in Fig. 2.

The above interpretation is supported by the following calculation. We split $A(x_i, x_e; t)$ into four pieces, $A_{\mu\nu}(x_i, x_e; t) = \langle \psi^\dagger_\mu(x_i, 0)\psi_\nu(x_e, t) + \psi_\nu(x_e, t)\psi^\dagger_\mu(x_i, 0)\rangle_w$, where $\mu, \nu = +, -$. At $k_B T \gtrsim \epsilon$ and for $x_e \in [x_i, L - x_i]$, we find that among the pieces, A_{++} dominantly determines $G_{\rm int}$. For general t, $A_{++}(x_i, x_e; t)$ is given by $(\pi a)^{-1} F(x_0) \times e^{i[k_F + \pi/(2L)]x_-}{\rm Re}[e^{i\pi x_0/(2L)} B(x_i, x_e; t)]$. Here, $F(x_0) = \langle e^{i\pi x_0 N/L}\rangle_w$ comes from the zero mode, $B(x_i, x_e; t) = [K(x_- - vt)]^{c_+^2}[K(-x_- - vt)]^{c_-^2}[K(-x_+ - vt)K(x_+ - vt)]^{c_+c_-}|K(2x)K(2y)|^{-c_+c_-}$ is the plasmon contribution, $x_\pm = x_e \pm x_i$, $x_0 = x_- - g^{-1}vt$, and $K(z) = (1 - e^{-\pi a/L})(1 - e^{(iz-a)\pi/L})^{-1} e^{-4\sum_{q>0}\langle b^\dagger_q b_q\rangle_w (\pi/qL)\sin^2(qz/2)}$. The plasmon modes contribute to A_{++} whenever one of the arguments of K's constituting B vanishes, since $K(z)$ rapidly decreases with increasing $|z|$ (mod$2L$) at $k_B T \gtrsim \epsilon$. Among those times, the most important contribution comes from $t_{\rm dire}$ and $t_{\rm boun}$ ($c_+ > c_-$), which are the two shortest arrival times of the blue mode at x_e.

For x_e around the nth recombination point, where the zero mode recombines with the blue after the round trip n times, $A_{++}(x_i, x_e; t_{\rm dire})$ is found to be proportional to

$$e^{-\ell^{-1}_{\phi,T}[(x_e - x_i)(g+1/g)/2 - vt_{\rm dire} - 2gL[(x_e - x_i - vt_{\rm dire}/g)/2L]^2]} \times e^{-\ell^{-1}_{\phi,T}[2gL[(x_e - x_i - vt_{\rm dire}/g)/2L]^2 + 2gn(x_e - x_i - vt_{\rm dire}/g)]}.$$

Here, we have used the approximation of $\langle b^\dagger_q b_q\rangle_w \propto 1/q$ in $K(z)$, which is valid for $k_B T \gtrsim \epsilon$. The second exponential factor comes from the zero mode while the first exponential factor describes the overlap between the blue and red plasmon modes. Note that in the exponents, the terms quadratic in $x_e - x_i$ cancel with each other while the linear terms survive. From these linear terms, we find that the coherence length $\ell_\phi(n)$ is given by

$$\ell^{-1}_\phi(n) = \ell^{-1}_{\phi,T} + \ell^{-1}_{\phi,\rm spinless}(n),$$
$$\ell^{-1}_{\phi,\rm spinless}(n) = \ell^{-1}_{\phi,T}\left[\frac{g^{-1} + g - 2}{2} - 2n(1 - g)\right], \quad (2)$$
$$\ell_{\phi,T} = \frac{\hbar v}{\pi k_B T}.$$

The thermal coherence length $\ell_{\phi,T}$ comes from the thermal smearing by F_T, while $\ell_{\phi,\rm spinless}(n)$ comes from the interaction effects; in the noninteracting case of $g = 1$, $\ell^{-1}_{\phi,T}$ still appears, while $\ell^{-1}_{\phi,\rm spinless}(n)$ (thus coherence revival and multiple coherence lengths) disappears. The proper values of n and the region where $\ell_\phi(n)$ is applied depend on g and

x_i. For $x_i \lesssim gL/(2-2g)$ [see Fig. 2], n runs over $0, 1, \ldots, n_{\max}$, where $n_{\max}$ is the largest integer smaller than $0.5 + (g^{-1} - 1)(L - 2x_i)/(2L)$, and $\ell_\phi(n)$ applies to the range of $2n - 1 \lesssim (g^{-1} - 1)(x_e - x_i)/L \lesssim 2n + 1$. Equation (2) is in excellent agreement with the calculation of $G_{\rm int}$ for various values of g and T (Fig. 3). The interaction-induced dephasing in Eq. (2) is caused by the excitations within energy window of $\sim \pi k_B T$, as the tail of the modes, which determines the overlap between the modes, decays exponentially with the rate of $l^{-1}_{\phi,\rm spinless} \propto \pi k_B T$. We remark that the coherence in the finite wire follows the infinite case only around the injection position, as the coherence length of the infinite wire [6] is equal to $\ell_\phi(n=0)$ in Eq. (2), and that $\ell_\phi(n) \propto T^{-1}$ as in other one dimensional systems [1–3,6].

From the fact that $\ell_\phi(n)$ is negative in the region where the revival occurs, we find that the condition for the occurrence of the revival is $\ell^{-1}_{\phi,\rm spinless}(n_{\max}) < 0$. For $x_i \lesssim L/4$, for instance, this condition results in $g \lesssim 1/3$. When the pure thermal effect of $\ell_{\phi,T}$ is factored out as in $G_{\rm int} e^{|x_e - x_i|/\ell_{\phi,T}}$, the coherence revival becomes more pronounced (see the insets of Figs. 2 and 3).

Spinful case.—In the spinful case, the spin mode moves slower than the charge modes by the factor g, showing the spin-charge separation [11], and the interaction is effectively weaker than the spinless case, as its number of states is 2 times larger. As a result, for $k_B T \gtrsim \epsilon$, ϵ here being the level spacing of the charge plasmons, we find that Eq. (2) is modified into

$$\begin{aligned} \ell_\phi^{-1}(n) &= \ell^{-1}_{\phi,T} + \ell^{-1}_{\phi,\rm ch}(n) + \ell^{-1}_{\phi,\rm sp}, \\ \ell^{-1}_{\phi,\rm ch}(n) &= \ell^{-1}_{\phi,T}\left[\frac{g^{-1} + g - 2}{4} - 2n(1-g)\right], \\ \ell^{-1}_{\phi,\rm sp} &= \ell^{-1}_{\phi,T}\frac{g^{-1} - 1}{2}. \end{aligned} \tag{3}$$

Here, $\ell_{\phi,\rm ch}$ comes from the dynamics of the charge modes and corresponds to $\ell_{\phi,\rm spinless}$, while $\ell_{\phi,\rm sp}$ shows the dephasing by the spin-charge separation. For $x_i/L \lesssim g/(1-g)$, $\ell_\phi(n)$ in Eq. (3) is applied to $2n - 1 \lesssim (g^{-1} - 1)(x_e - x_i)/(2L) \lesssim 2n + 1$, where n runs over $0, 1, \ldots, n_{\max}$ and $n_{\max} \simeq (g^{-1} - 1)(L - 2x_i)/(4L)$. The revival of the coherence appears at $x_e = L - x_i$ for $g \lesssim 1/5$, when $x_i \lesssim L/4$. Note that the revival of the coherence with multiple coherence lengths due to the charge modes can be singled out by measuring $G_{\rm int} e^{|x_e - x_i|(\ell^{-1}_{\phi,T} + \ell^{-1}_{\phi,\rm sp})}$.

Conclusion.—We have shown that the interplay of the interaction and the finite-size effect, such as the dynamics of the electron fractionalization (into the plasmon modes and the zero mode) under the boundary bouncing, can cause nontrivial behavior of electron coherence in a finite-size system, which is drastically different from the infinite case. Our finding may motivate further research activities towards the understanding of coherence of interacting particles in various systems [14–17].

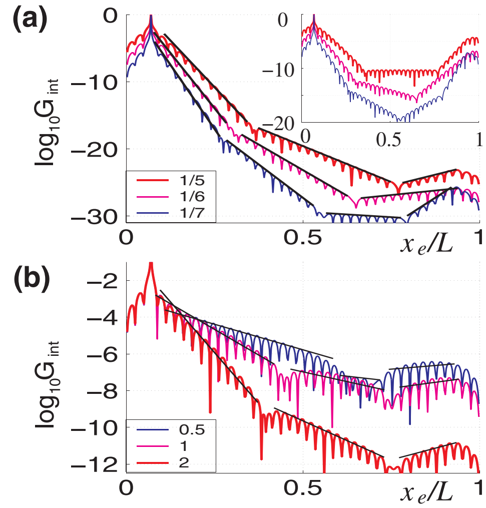

FIG. 3 (color online). Dependence on temperature and interaction strength. The same as in Fig. 2(a) except for different values of $k_B T$ and g. (a) $g = 1/5$, $1/6$, and $1/7$ from top to bottom, while $k_B T = 5\epsilon$ is common. (b) $k_B T = 0.5\epsilon$, ϵ, and 2ϵ from top to bottom, while $g = 1/5$. The black lines represent the slopes obtained from $\ell_\phi(n)$ in Eq. (2).

We thank M. Bockrath and A. Braggio for discussion. This work was supported by KRF (2006-331-C00118).

*hssim@kaist.ac.kr

[1] A. E. Hansen, A. Kristensen, S. Pedersen, C. B. Sørensen, and P. E. Lindelof, Phys. Rev. B **64**, 045327 (2001).
[2] P. Roulleau *et al.*, Phys. Rev. Lett. **100**, 126802 (2008).
[3] G. Seelig and M. Büttiker, Phys. Rev. B **64**, 245313 (2001).
[4] K.-V. Pham, M. Gabay, and P. Lederer, Phys. Rev. B **61**, 16 397 (2000).
[5] H. Steinberg *et al.*, Nature Phys. **4**, 116 (2008).
[6] K. Le Hur, Phys. Rev. Lett. **95**, 076801 (2005).
[7] B. Trauzettel, I. Safi, F. Dolcini, and H. Grabert, Phys. Rev. Lett. **92**, 226405 (2004).
[8] A. V. Lebedev, A. Crépieux, and T. Martin, Phys. Rev. B **71**, 075416 (2005).
[9] Y. Meir and N. S. Wingreen, Phys. Rev. Lett. **68**, 2512 (1992).
[10] For $x_e = x_i$, $I_{\rm int}$ is equivalent to the expression derived in J. König and Y. Gefen, Phys. Rev. Lett. **86**, 3855 (2001).
[11] T. Giamarchi, *Quantum Physics in One Dimension* (Oxford University, New York, 2004).
[12] M. Fabrizio and A. O. Gogolin, Phys. Rev. B **51**, 17 827 (1995).
[13] A. E. Mattsson, S. Eggert, and H. Johannesson, Phys. Rev. B **56**, 15 615 (1997).
[14] I. Neder, M. Heiblum, Y. Levinson, D. Mahalu, and V. Umansky, Phys. Rev. Lett. **96**, 016804 (2006).
[15] S.-C. Youn, H.-W. Lee, and H.-S. Sim, Phys. Rev. Lett. **100**, 196807 (2008).
[16] I. Neder, and E. Ginossar, Phys. Rev. Lett. **100**, 196806 (2008).
[17] E. V. Sukhorukov and V. V. Cheianov, Phys. Rev. Lett. **99**, 156801 (2007).